Spectral representation of the three-body Coulomb problem: Perspectives for highly doubly excited states of helium

Johannes Eiglsperger
Physik Department, Technische Universität München, 85747 Garching, Germany

Bernard Piraux
Laboratoire de Physique Atomique, Moléculaire et Optique (PAMO), Université catholique de Louvain, 1348 Louvain-la-Neuve, Belgium

Javier Madroñero
Physik Department, Technische Universität München, 85747 Garching, Germany and Laboratoire de Physique Atomique, Moléculaire et Optique (PAMO), Université catholique de Louvain, 1348 Louvain-la-Neuve, Belgium

(Received 9 April 2009; published 21 August 2009)

We present a spectral method of configuration-interaction type for three-dimensional helium which combines the complex rotation method with an appropriate expansion of the atom wave function in a basis of products of Coulomb-Sturmian functions of the electron radial coordinates with *independent* dilation parameters for the two electrons and bipolar spherical harmonics of the angular coordinates. The matrix elements of the kinetic energy and of the electron-nucleus interaction term are calculated using Gauss-Laguerre integration techniques. A combination of Gauss-Laguerre integration techniques with the generalized Wigner-Eckart theorem and recurrence relations allows an efficient and stable calculation of the matrix elements of the electron-electron interaction. The freedom of the choice of the dilation parameters permits us to access highly excited states with rather small sizes of the basis. Highly doubly excited states up to the tenth ionization threshold of singlet and triplet S states of helium are presented.

DOI: 10.1103/PhysRevA.80.022511 PACS number(s): 32.30.−r, 02.70.Hm, 31.15.ac

I. INTRODUCTION

As was first realized through an experiment by Madden and Codling [1], doubly excited states of helium cannot in general be described by a simple model based on independent-particle angular momentum quantum numbers Nl_1nl_2. Since then, the regime near to the double ionization threshold represents a paradigm for electron correlations in atomic systems and has therefore attracted the continuous interest of both theoreticians and experimentalists. A large amount of theoretical and computational effort has been invested in the attempt to improve our understanding of electron correlations in two-electron atoms, see, e.g., [2–7] and references therein.

Doubly excited states of two-electron atoms are organized in series converging toward the single-ionization thresholds (SITs) I_N of $\mathrm{He}(N)^+$ states. The inherent strongly correlated nature of doubly excited states requires the introduction of new classification schemes, e.g., consisting of the approximate quantum numbers (n,N,K,T) [8,9]. Starting from the fourth SIT, members of higher-lying series interfere with lower series. Above the eighth ionization series the widths of the resonances can be larger than their separation [4,10]. In the recent years an improvement of measurement techniques has allowed a detailed examination of doubly excited states converging up to the $N=16$ threshold of He [10–12]. From the theoretical side, close to the double ionization threshold the number of open channels increases dramatically. Therefore, currently available full three-dimensional (3D) approaches require rather large basis sets for the representation of the associated eigenvalue problem. Simplified one-dimensional (1D) models or the s^2 model [13–18] of the 3D atom reduce significantly the calculation difficulties. However, the former models may underestimate the decay rates of the resonances by orders of magnitude [19], and the latter cannot associate computed states to semiclassical configurations such as the frozen planet [20] or the asymmetric stretch configuration, which are essential for the discussion of Ericson fluctuations in photoionization cross sections [12,21]. The planar (2D) helium model [21–23], in which the dynamics are confined to a two-dimensional configuration space, allows a qualitative description of the helium spectrum near the total fragmentation threshold for any value of the total angular momentum L, which enables one to describe the driven system in the framework of Floquet theory, and, in particular, a computation of the triplet P-state spectrum up to the 23rd threshold. For the treatment of the full 3D problem there are mainly two classes of approaches. On the one hand, there is the explicitly correlated (EC) approach [24] in which the interelectronic distance r_{12} is an explicit coordinate. The expansion in functions of perimetric coordinates, which is of EC type, allows at present a very accurate description of the singlet P-state spectrum up to the $N=17$ threshold [12]. An EC basis expansion in terms of Sturmian functions [25,26] of perimetric coordinates leads to a banded matrix representation of the Hamiltonian, and all its matrix elements are computed analytically. This allows the treatment of matrices of rather large size and accurate calculation of the energy and width of singly and doubly excited states. However, this method is essentially limited to small total angular momenta $L=0,1,2$ due to the dramatic increase in selection rules with L. This also imposes a limitation for the treatment of helium

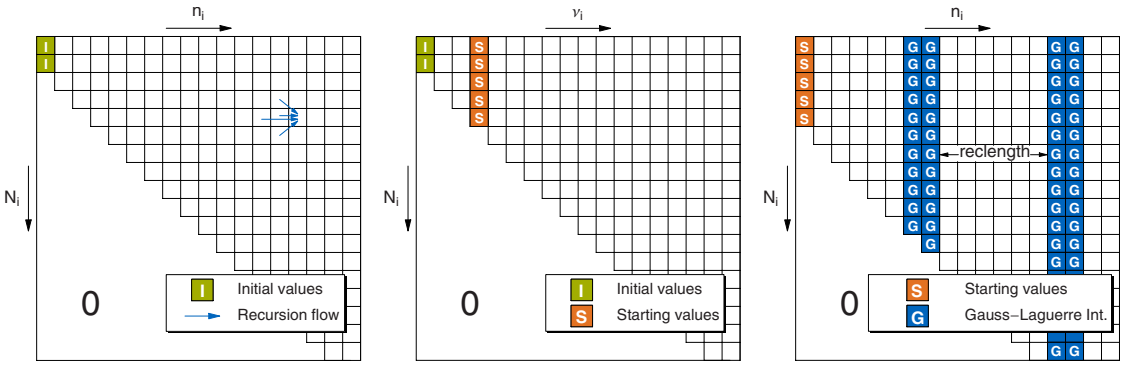

FIG. 1. (Color online) (Left) Coefficients for $\nu_i=\lambda_i+1$: initial values computed via Eq. (29) are marked by the letter *I*. Representative for all coefficients the recursion flow for the computation of one matrix element is indicated with arrows. (Center) Coefficients for $n_i=l_i+1$: initial values computed via Eq. (29) are marked by the letter *I*. The starting values for the coefficients with $\nu_i=\lambda_i+4$ are marked by the letter *S*. (Right) Coefficients for $\nu_i\neq\lambda_i+1$: as a representative the coefficients with $\nu_i=\lambda_i+4$ are pictured. The starting values characterized by the letter *S* correspond to the values marked by an *S* in the center picture of this figure. The values for the restart of the recursion are highlighted by *G*. All coefficients $(\nu_i,n_i|N_i)$ with $N_i>\nu_i+n_i$ are equal to zero.

under periodic driving and multiphoton single and double ionization. On the other hand, there are the spectral methods of configuration-interaction (CI) type, in which the wave function is expanded in single-particle wave functions and r_{12} is not an explicit coordinate. Within these methods the computation of states with $L\geq 3$ does not pose any additional difficulties and are frequently used for the description of few-photon ionization processes [7,27–32] where highly doubly excited states do not play a fundamental role. However, up to now, methods of this type have not been applied to the computation of highly doubly excited states. These states are expected to play an important role in the ionization by low-frequency intense laser pulses [33,34] or in the description of nondispersive two-electron wave packets [23]. However, an accurate theoretical treatment of such a problem defines a formidable theoretical and numerical challenge due to the field-induced coupling of several total angular momenta and the dimensions of the matrices associated to single total angular momenta. Note, however, that a 3D *ab initio* fully numerical treatment of the ionization of helium in the low-frequency regime is available [35] and has been already used to give a rather qualitative description of the correlations in the ionization process of helium from the ground state by a 780 nm laser pulse of peak intensity $(0.275-14.4)\times 10^{14}$ W/cm^2. However, due to the difficulty to extract physical information from this grid approach and its high requirements concerning computational resources, an accurate spectral approach to this problem becomes even more desirable.

In this paper, we demonstrate that highly doubly excited states may be computed within a CI approach. For this purpose, we extend the approach presented in [7] in which the radial part of the wave function is expanded in terms of products of Coulomb-Sturmian functions with independent dilation parameters for each electron and coupled spherical harmonics for the angular coordinates. In particular, we develop an efficient method for the computation of the matrix elements of the *e*-*e* interaction term. Our method combines the Gauss-Laguerre (GL) integration techniques together with the generalized Wigner-Eckart theorem and recursion relations [36,37], which leads to a significant reduction in computation time. This is crucial for the study of the highly excited regime of the spectrum, of which the accurate description requires rather large matrices, though these are considerably smaller than those used in state-of-the-art methods. The latter is achieved by an appropriate choice of the dilation parameters which allows an efficient description of rather wide regions of the spectrum.

In addition, this approach is equally valid for the description of any total angular momentum manifold. Therefore, besides the study of the fundamental problem of the understanding of the regime close to the double ionization threshold of two-electron atoms, our approach also provides perspectives for the treatment of the interaction of helium with low-frequency intense laser pulses or for the formation of nondispersive wave packets.

The paper is organized as follows: in Secs. II and III we outline our theoretical and numerical setups, respectively. Section IV presents results for $L=0$ states for singlet and triplet symmetries up to the tenth ionization threshold. Section V concludes the paper. Unless stated otherwise, atomic units are used throughout this document.

II. THEORETICAL APPROACH

A. Spectral method

The nonrelativistic Hamiltonian H for the helium atom, under the assumption of an infinitely heavy nucleus, reads as

$$H=\frac{\vec{p}_1^{\,2}}{2}+\frac{\vec{p}_2^{\,2}}{2}-\frac{2}{r_1}-\frac{2}{r_2}+\frac{1}{r_{12}}, \tag{1}$$

with the interelectronic distance

$$\frac{1}{r_{12}}=\frac{1}{|\vec{r}_1-\vec{r}_2|}, \tag{2}$$

and $\vec{r}_1$, $\vec{r}_2$, $\vec{p}_1$, and $\vec{p}_2$ the position and momentum vectors of electrons 1 and 2, respectively. The eigenstate wave function of the helium atom with a total angular momentum L of

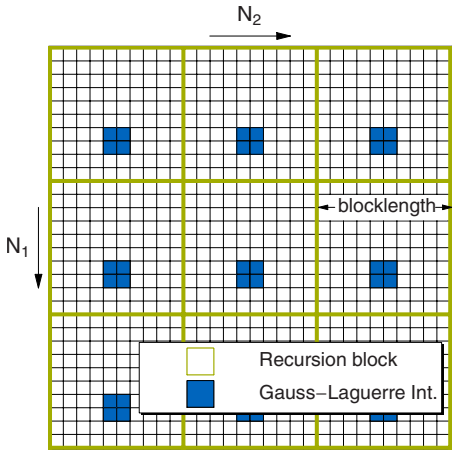

FIG. 2. (Color online) $\mathcal{G}_{N_1,N_2}$: a schematic depiction for the computation of matrix $\mathcal{G}$. The matrix is decomposed in subblocks of dimension $\mathfrak{B}$. Within each of these subblocks a set of four initial values is computed using GL integration from which the rest of the matrix elements can be calculated employing Eqs. (31) and (32).

projection M and total energy E_α satisfies the time-independent Schrödinger equation

$$(H - E_\alpha)\Psi_\alpha^{L,M}(\vec{r}_1,\vec{r}_2) = 0. \tag{3}$$

In our approach [7,38], which is of CI type, the solutions to Eq. (3) is expanded as follows:

$$\Psi_\alpha^{L,M}(\vec{r}_1,\vec{r}_2) = \sum_{l_1,l_2}\sum_{s}\sum_{n_1,n_2} \psi^{l_1,l_2,L,M}_{k_{1s},k_{2s},n_1,n_2,\alpha}\beta^{l_1,l_2}_{n_1,n_2} \times \mathcal{A}\frac{S^{(k_{1s})}_{n_1,l_1}(r_1)}{r_1}\frac{S^{(k_{2s})}_{n_2,l_2}(r_2)}{r_2}\Lambda^{L,M}_{l_1,l_2}(\hat{r}_1,\hat{r}_2), \tag{4}$$

where $\psi^{l_1,l_2,L,M}_{k_{1s},k_{2s},n_1,n_2,\alpha}$ is the expansion coefficient and $\beta^{l_1,l_2}_{n_1,n_2} = 1 + (1/\sqrt{2} - 1)\delta_{n_1,n_2}\delta_{l_1,l_2}$ controls the redundancy that might occur within the basis due to symmetrization. The symmetry or antisymmetry of the spatial wave function, as required by the Pauli principle, is ensured by a projection onto either singlet or triplet states via the operator

$$\mathcal{A} = \frac{1 + \epsilon P}{\sqrt{2}}, \tag{5}$$

where the operator P exchanges both electrons and ϵ takes values of $+1$ or -1 for singlet or triplet states, respectively. The radial one-electron functions $S^{(k)}_{n,l}(r)$ are the Coulomb-Sturmian functions [25,26] defined for a given angular momentum l and radial index n by

$$S^{(k)}_{n,l}(r) = N^{(k)}_{n,l}(2kr)^{l+1}L^{(2l+1)}_{n-l-1}(2kr)\exp(-kr), \tag{6}$$

where k is a dilation parameter and $L^{(2l+1)}_{n-l-1}(2kr)$ is a Laguerre polynomial. The normalization constant $N^{(k)}_{n,l}$ given by

$$N^{(k)}_{n,l} = \sqrt{\frac{k}{n}}\left(\frac{(n-l-1)!}{(n+l)!}\right)^{1/2} \tag{7}$$

is chosen in order to satisfy the overlap condition

TABLE I. Singlet state resonances below I_2: our results on the left are compared with the results of [3]. The dimension of the matrices used to obtain these data was $n=11472$ and $p=8304$, respectively. The data presented were subject to a stability analysis with respect to varying values of the complex rotation angle θ. By increasing the excitation of the outer electron (downwards in the table), the convergence improves.

$-\mathrm{Re}(E_{i,\theta})$	$-\mathrm{Im}(E_{i,\theta})$	$-\mathrm{Re}(E_{i,\theta})$	$-\mathrm{Im}(E_{i,\theta})$
This work		Bürgers *et al.* [3]	
0.77787	0.00227	0.777867636	0.002270653
0.6219	0.0001	0.621927254	0.000107818
0.589895	0.000681	0.589894682	0.000681239
0.54808	0.00004	0.548085535	0.000037392
0.544882	0.000246	0.544881618	0.000246030
0.527715	0.000023	0.527716640	0.000023101
0.526687	0.000109	0.526686857	0.000109335
0.518103	0.000015	0.518104252	0.000014894
0.517641	0.000057	0.517641112	0.000056795
0.512763	0.000010	0.512763242	0.000009970
0.5125135	0.0000330	0.512513488	0.000032992
0.5094833	0.0000069	0.509483569	0.000006918
0.5093327	0.0000208	0.509332686	0.000020795
0.507324	0.000005	0.507324340	0.000004959
0.5072258	0.0000139	0.507225835	0.000013936
0.505827	0.000004	0.505827143	0.000003657
0.5057591	0.0000098	0.505759104	0.000009790
0.5047463	0.0000028	0.504746388	0.000002766
0.5046973	0.0000072		
0.5039403	0.0000021		
0.5039040	0.0000054		
0.5033238	0.0000016		
0.5032958	0.0000042		
0.5028415	0.0000013		
0.5028196	0.0000033		
0.5024570	0.0000011		
0.5024395	0.0000026		
0.5021456	0.0000009		
0.5021314	0.0000021		
0.5018898	0.0000007		
0.5018782	0.0000018		
0.5016675	0.0000015		

$$\int_0^\infty dr S^{(k)}_{n,l}(r)S^{(k)}_{n,l}(r) = 1. \tag{8}$$

With this, the orthogonality relation for the Sturmian functions reads

$$\int_0^\infty dr S^{(k)}_{n,l}(r)\frac{1}{r}S^{(k)}_{n',l}(r) = \frac{k}{n}\delta_{nn'}. \tag{9}$$

The radial index n of the Sturmian functions is a positive integer satisfying $n \geq l+1$. The angular part of expansion (4)

TABLE II. Triplet state resonances below I_2: our results on the left are compared with the results of [3]. The dimension of the matrices used to obtain these data was $n=11472$ and $p=7936$, respectively. The data presented were subject to a stability analysis with respect to varying values of the complex rotation angle θ. The last few resonances are exclusively members of the $K=1$ series.

$-\mathrm{Re}(E_{i,\theta})$	$-\mathrm{Im}(E_{i,\theta})$	$-\mathrm{Re}(E_{i,\theta})$	$-\mathrm{Im}(E_{i,\theta})$
This work		Bürgers *et al.* [3]	
0.60257751	0.00000332	0.602577505	0.000003325
0.55974655	0.00000010	0.559746626	0.000000130
0.54884086	0.00000155	0.548840858	0.000001547
0.53250532	0.00000006	0.532505349	0.000000072
0.528413972	0.000000772	0.528413972	0.000000771
0.52054918	0.00000004	0.520549199	0.000000041
0.518546375	0.000000429	0.518546375	0.000000428
0.51418035	0.00000002	0.514180356	0.000000025
0.513046496	0.000000260	0.513046496	0.000000260
0.510378167	0.000000017	0.510378174	0.000000016
0.509672798	0.000000169	0.509672798	0.000000169
0.50792515	0.00000001	0.507925149	0.000000011
0.507456056	0.000000116	0.507456056	0.000000116
0.506250076	0.000000007	0.506250079	0.000000008
0.505922151	0.000000083	0.505922151	0.000000082
0.505055338	0.000000005	0.505055341	0.000000006
0.504817014	0.000000061		
0.50399459	0.00000005		
0.503366094	0.000000035		
0.502875028	0.000000027		
0.502484067	0.000000022		
0.502167743	0.000000018		
0.501902040	0.000000015		

is expressed in terms of bipolar spherical harmonics [39],

$$\Lambda_{l_1,l_2}^{L,M}(\hat{r}_1,\hat{r}_2)=\sum_{m_1,m_2}\langle l_1,m_1,l_2,m_2|L,M\rangle Y_{l_1,m_1}(\hat{r}_1)Y_{l_2,m_2}(\hat{r}_2), \tag{10}$$

which couple the two individual angular momenta l_1 and l_2 in the L-S scheme. $Y_{l,m}$ denotes the spherical harmonics and $\langle l_1,m_1,l_2,m_2|L,M\rangle$ is a Clebsch-Gordon coefficient. In order to preserve parity, which is a good quantum number, the L-S coupled individual angular momenta of the electrons must satisfy $(-1)^L=(-1)^{l_1+l_2}$ [40]. To avoid redundancies in expansion (4), the orbital angular momenta are restricted to $l_1\leq l_2$, and if $l_1=l_2$ and $k_{1s}=k_{2s}$ to $n_1\leq n_2$.

Within a CI approach, the interelectronic distance $1/r_{12}$ is not directly accessible. Instead one has to exploit the multipole expansion of the electron-electron repulsion to get an expression for the interelectronic distance,

$$\frac{1}{r_{12}}=\sum_{q=0}^{\infty}\sum_{p=-q}^{q}\frac{4\pi}{2q+1}\frac{r_<^q}{r_>^{q+1}}Y_{q,p}^*(\hat{r}_1)Y_{q,p}(\hat{r}_2), \tag{11}$$

with $r_<=\min(r_1,r_2)$ and $r_>=\max(r_1,r_2)$.

TABLE III. Singlet state resonances below I_3: our results on the left are compared with the results of [3]. The dimension of the matrices used to obtain these data was $n=11744$ and $p=6951$, respectively. The data presented were subject to a stability analysis with respect to varying values of the complex rotation angle θ.

$-\mathrm{Re}(E_{i,\theta})$	$-\mathrm{Im}(E_{i,\theta})$	$-\mathrm{Re}(E_{i,\theta})$	$-\mathrm{Im}(E_{i,\theta})$
This work		Bürgers *et al.* [3]	
0.353538	0.001505	0.353538536	0.001504906
0.31745	0.00333	0.317457836	0.003329920
0.281073	0.000751	0.281072703	0.000750733
0.263388	0.001209	0.263388312	0.001209354
0.25737	0.00001	0.257371610	0.000010564
0.25597	0.00035	0.255972114	0.000350036
0.246635	0.000566	0.246634603	0.000565481
0.244324	0.000021	0.244324739	0.000021400
0.243824	0.000180	0.238524104	0.000318437
0.23853	0.00032	0.243824049	0.000179910
0.237310	0.000016	0.237311202	0.000017021
0.23715	0.00010	0.237147099	0.000102160
0.233900	0.000196	0.233898812	0.000196262
0.233172	0.000012	0.233173689	0.000012347
0.233122	0.000062	0.233121363	0.000062881
0.231002	0.000129	0.231001524	0.000129185
0.230531	0.000009	0.230531347	0.000008810
0.230520	0.000041	0.230519146	0.000041369
0.229065	0.000090	0.229064586	0.000089418
0.228744	0.000028	0.228744234	0.000028755
0.228741	0.000006	0.228741812	0.000006247
0.227706	0.000065	0.227705232	0.000064398
0.227482	0.000021	0.227481269	0.000020794
0.227474	0.000004	0.227473958	0.000004545
0.226715	0.000048	0.22671442	0.00004789
0.226552	0.000015	0.226551500	0.000015492
0.2265427	0.0000033	0.22654299	0.00000342
0.225971	0.000037		
0.225848	0.000012		
0.2258390	0.0000026		
0.225397	0.000029		
0.2253023	0.0000092		
0.2252943	0.0000020		
0.224945	0.000023		
0.2248710	0.0000073		
0.2248640	0.0000016		
0.224584	0.000018		
0.2245242	0.0000059		

TABLE III. (*Continued.*)

$-\mathrm{Re}(E_{i,\theta})$	$-\mathrm{Im}(E_{i,\theta})$	$-\mathrm{Re}(E_{i,\theta})$	$-\mathrm{Im}(E_{i,\theta})$
This work		Bürgers *et al.* [3]	
0.2245181	0.0000013		
0.2242898	0.0000152		
0.2242413	0.0000049		
0.22423593	0.00000110		
0.2240475	0.0000126		
0.2240074	0.0000040		
0.22400277	0.00000092		
0.223845	0.000010		
0.223811	0.000003		
0.2238080	0.0000008		

In general, the CI expansions involving Coulomb-Sturmian functions use the same dilation parameter k for all Coulomb-Sturmian functions, which is equivalent to setting $k_{1s}=k_{2s}\equiv k$ and $s=1$ in expansion (4). Furthermore, for each pair of (l_1,l_2), the same number N of Coulomb-Sturmian functions $S^{(k)}_{n_1,l_1}(r_1)$ with $l_1+1\leq n_1\leq l_1+N$ and $S^{(k)}_{n_2,l_2}(r_2)$, with $l_2+1\leq n_2\leq l_2+N$ is taken into account. In contrast our approach is constructed in order to allow the dilation parameter and the number of Coulomb-Sturmian functions associated to one electron to be different from those attributed to the other electron. This leads to the introduction of a set of Coulomb-Sturmian functions $\{S^{(k_{1s})}_{n_1,l_1}(r_1),S^{(k_{2s})}_{n_2,l_2}(r_2)\}$ associated to electron one and two, which is characterized by the combination $[k_{1s},N^{\min}_{1s},N^{\max}_{1s},k_{2s},N^{\min}_{2s},N^{\max}_{2s}]$, with $l_1+N^{\min}_{1s}\leq n_1\leq l_1+N^{\max}_{1s}$ and $l_2+N^{\min}_{2s}\leq n_2\leq l_2+N^{\max}_{2s}$. Moreover, more than one and different sets—labeled by the subscript s—may be selected for any angular configuration (l_1,l_2).

By choosing appropriate sets of Coulomb-Sturmian functions the description of a given energy regime, i.e., below a certain ionization threshold, is possible with a rather small number of basis functions.

B. Complex rotation

The electron-electron interaction in helium couples different channels of the noninteracting two-electron dynamics and gives rise to resonance states embedded in the continua above the first SIT. To extract the resonance states and their decay rates we use complex rotation (or "dilation") [41–45], which was shown to be applicable for the Coulomb potential in [46].

The complex dilation of any operator by an angle θ is mediated by the nonunitary complex rotation operator

$$R(\theta)=\exp\left(-\theta\frac{\vec{r}\cdot\vec{p}+\vec{p}\cdot\vec{r}}{2}\right), \tag{12}$$

where $\vec{r}$ and $\vec{p}$ represent the six component vector made up of $\vec{r}_1$, $\vec{r}_2$ and $\vec{p}_1$, $\vec{p}_2$, respectively. Rotation of the position and

TABLE IV. Triplet state resonances below I_3: our results on the left are compared with the results of [3]. The dimension of the matrices used to obtain these data was $n=11744$ and $p=6760$, respectively. The data presented were subject to a stability analysis with respect to varying values of the complex rotation angle θ.

$-\mathrm{Re}(E_{i,\theta})$	$-\mathrm{Im}(E_{i,\theta})$	$-\mathrm{Re}(E_{i,\theta})$	$-\mathrm{Im}(E_{i,\theta})$
This work		Bürgers *et al.* [3]	
0.28727713833	0.00001491439	0.287277138	0.000014914
0.270283613	0.000023307	0.270283614	0.000023308
0.258133977	0.000009749	0.258133976	0.000009748
0.24996463	0.00000678	0.249964616	0.000006789
0.249000427	0.000006842	0.249000418	0.000006848
0.24480749	0.00000581	0.244807489	0.000005801
0.24031449	0.00000348	0.240314494	0.000003490
0.23969689	0.00000460	0.239696887	0.000004600
0.23767221	0.00000358	0.237672213	0.000003578
0.23496955	0.00000203	0.234969582	0.000002042
0.23456903	0.00000306	0.234569038	0.000003061
0.23343332	0.00000233	0.233433327	0.000002322
0.231692091	0.000001298	0.231692116	0.000001300
0.23142164	0.00000211	0.231421646	0.000002100
0.23071908	0.00000158	0.230719088	0.000001578
0.229535681	0.000000880	0.229535701	0.000000880
0.229345777	0.000001492	0.229345782	0.000001491
0.228880000	0.000001117	0.228880000	0.000001117
0.228040858	0.000000620	0.228040873	0.000000623
0.227902911	0.000001092	0.227902914	0.000001091
0.22757745	0.00000082	0.2275778	0.0000008
0.226961937	0.000000455	0.226962	0.000001
0.226858802	0.000000823	0.226859	0.000001
0.22662254	0.00000061		
0.22615767	0.00000034		
0.22607865	0.00000064		
0.225901438	0.000000473		
0.225542108	0.000000264		
0.225480290	0.000000496		
0.225343862	0.000000371		
0.225060490	0.000000209		
0.225011251	0.000000400		
0.224903928	0.000000297		
0.224676582	0.000000169		
0.224636744	0.000000323		
0.224550762	0.000000241		
0.224365627	0.000000137		
0.224332952	0.000000265		

TABLE IV. (*Continued.*)

$-\mathrm{Re}(E_{i,\theta})$	$-\mathrm{Im}(E_{i,\theta})$	$-\mathrm{Re}(E_{i,\theta})$	$-\mathrm{Im}(E_{i,\theta})$
This work		Bürgers *et al.* [3]	
0.224262980	0.000000198		
0.224110242	0.000000113		
0.224083116	0.000000221		
0.22387516	0.00000017		

momentum operators in the complex plane according to

$$\vec{r} \to R(\theta)\vec{r}R(-\theta) = \vec{r}\exp(\imath\theta),$$

$$\vec{p} \to R(\theta)\vec{p}R(-\theta) = \vec{p}\exp(-\imath\theta), \tag{13}$$

transforms Hamiltonian (1) into a non-Hermitian operator with complex eigenvalues given by

$$H(\theta) = \left(\frac{\vec{p}_1^2 + \vec{p}_2^2}{2}\right)\exp(-2\imath\theta) - \left(\frac{2}{r_1} + \frac{2}{r_2} - \frac{1}{r_{12}}\right)\exp(-\imath\theta). \tag{14}$$

However, the spectrum of the rotated Hamiltonian has the following important properties [42,44,46]:

(1) The bound spectrum of H is invariant under the complex rotation.

(2) The continuum states are located on half lines rotated by an angle -2θ around the ionization thresholds of the unrotated Hamiltonian into the lower half of the complex plane. In the specific case of the unperturbed 3D helium Hamiltonian (1) the continuum states are rotated around the SIT $I_N = -2/N^2$ [47], with $N \in \mathbb{N}$.

(3) There are isolated complex eigenvalues $E_{i,\theta} = E_i - \imath\Gamma_i/2$ in the lower half plane corresponding to resonance states. These are stationary under the variation of θ provided that the dilation angle is large enough to uncover their positions on the Riemannian sheets of the associated resolvent [47,48]. The associated resonance eigenfunctions are square integrable [45], in contrast to the resonance eigenfunctions of the unrotated Hamiltonian. The latter are asymptotically diverging outgoing waves [45,49,50].

The eigenstates of $H(\theta) = R(\theta)HR(-\theta)$,

$$H(\theta)|\Psi_{i,\theta}^{L,M}\rangle = E_{i,\theta}|\Psi_{i,\theta}^{L,M}\rangle, \tag{15}$$

are normalized for the scalar product

$$\langle\Psi_{j,-\theta}^{L,M}|\Psi_{i,\theta}^{L,M}\rangle = \delta_{ij} \tag{16}$$

and satisfy the closure relation

$$\sum_i |\Psi_{i,\theta}^{L,M}\rangle\langle\Psi_{i,-\theta}^{L,M}| = 1. \tag{17}$$

TABLE V. Singlet state resonances below I_4: our results on the left are compared with the results of [3]. The dimension of the matrices used to obtain these data was $n=11744$ and $p=6576$, respectively. The data presented were subject to a stability analysis with respect to varying values of the complex rotation angle θ. Some more converged resonances have been obtained but are not displayed for lack of space.

$-\mathrm{Re}(E_{i,\theta})$	$-\mathrm{Im}(E_{i,\theta})$	$-\mathrm{Re}(E_{i,\theta})$	$-\mathrm{Im}(E_{i,\theta})$
This work		Bürgers *et al.* [3]	
0.200990	0.000970	0.200989572	0.000969178
0.18783	0.00246	0.187834626	0.002458380
0.168261	0.001085	0.168261328	0.001086186
0.165734	0.000605	0.165734021	0.000605047
0.15691	0.00138	0.156904051	0.001377256
0.15083	0.00032	0.150824382	0.000320293
0.147267	0.000412	0.147266965	0.000416449
0.145400	0.000809	0.145397764	0.000808943
0.142603	0.000169	0.142602474	0.000169806
0.141066	0.000010	0.141064156	0.000011739
0.1398403	0.0002400	0.139840342	0.000239815
0.139190	0.000475	0.139189490	0.000475268
0.137686	0.000091	0.137685346	0.000092512
0.137088	0.000002	0.137088229	0.000002490
0.135728	0.000160	0.135728512	0.000160253
0.135439	0.000290	0.135437398	0.000289889
0.134551	0.000049	0.134551108	0.000049711
0.134229	0.000003	0.134228598	0.000002711
0.133141	0.000110	0.133141846	0.000111361
0.132997	0.000184	0.132996200	0.000183914
0.1324519	0.0000233	0.132451935	0.000023393
0.1322133	0.0000030	0.132212660	0.000003293
0.131396	0.000080	0.131396547	0.000080331
0.131320	0.000121	0.131319807	0.000120624
0.1309991	0.0000058	0.130999124	0.000005799
0.1307731	0.0000031	0.130772717	0.000003289
0.130160	0.000059	0.130160039	0.000059877
0.130121	0.000080	0.130120051	0.000080068
0.1299935	0.0000027	0.129993447	0.000002704
0.1297182	0.0000028	0.129717890	0.000002986
0.129251	0.000046	0.129251251	0.000046022
0.129323	0.000033	0.129322969	0.000033799
0.129225	0.000058	0.129224756	0.000057660
0.1289253	0.0000025	0.128925097	0.000002597
0.128777	0.000053	0.128776594	0.000054043
0.1285627	0.0000361	0.128562811	0.000036493
0.128552	0.000041	0.128551852	0.000041001
0.12831547	0.00000213	0.128315304	0.000002218
0.1282625	0.0000396	0.128262189	0.000039756
0.1280296	0.0000312	0.128029833	0.000031311
0.1280257	0.0000274	0.128025335	0.000027559
0.1278368	0.0000018	0.127836684	0.000001881

TABLE V. (*Continued.*)

$-\mathrm{Re}(E_{i,\theta})$	$-\mathrm{Im}(E_{i,\theta})$	$-\mathrm{Re}(E_{i,\theta})$	$-\mathrm{Im}(E_{i,\theta})$
This work		Bürgers *et al.* [3]	
0.1278159	0.0000270	0.12781573	0.00002743
0.1276101	0.0000257	0.127610012	0.000025737
0.1276056	0.0000198	0.127605478	0.000019886
0.12745445	0.00000154	0.127454353	0.000001595
0.1274462	0.0000196	0.1274461	0.0000200
0.1272715	0.0000206	0.127271404	0.000020669
0.1272676	0.0000153	0.127267459	0.000015312
0.1271443	0.0000013	0.127144218	0.000001356
0.1271418	0.0000148	0.1271415	0.0000152
0.1269945	0.0000164	0.1269944	0.0000166
0.1269913	0.0000123	0.1269912	0.0000123
0.1268895	0.0000116		
0.12688930	0.00000112	0.12688926	0.00000118

C. Matrix representation

After substituting $\Psi_{\alpha}^{L,M}$ in Eq. (3) by its expansion [Eq. (4)] and using the complex rotation method described previously, we obtain the following generalized eigenvalue problem:

$$\mathbf{H}_{\theta}\mathbf{\Psi}_{i,\theta} = E_{i,\theta}\,\mathbf{S}\mathbf{\Psi}_{i,\theta}, \tag{18}$$

where $\mathbf{\Psi}_{i,\theta}$ is the vector representation of the wave function $|\Psi_{i,\theta}\rangle$, $\mathbf{S}$ is the matrix representing the overlap, and $\mathbf{H}_{\theta}$ is the matrix associated with the rotated Hamiltonian. The calculation of matrix elements of $\mathbf{S}$ and $\mathbf{H}_{\theta}$ may be performed analytically, which becomes, however, cumbersome as soon as various sets of Coulomb-Sturmian functions with different dilation parameters are introduced. Alternatively GL integration [38,51] provides extremely accurate results for the matrix elements in Eq. (18) since the GL quadrature formula is exact in our case where all integrals to calculate involve products of polynomials and decreasing exponentials. In addition, the matrix elements of the overlap matrix $\mathbf{S}$, of the kinetic energy, and of the Coulomb interaction of the electrons with the nucleus can be computed efficiently with GL integration. The situation for the electron-electron repulsion is different: the computation of matrix elements associated with the $1/r_{12}$ term Eq. (11) involves the following radial double integral:

$$U = \int_0^{\infty} dr_1 \int_0^{\infty} dr_2 S_{\nu_1,\lambda_1}^{(\kappa_1)}(r_1) S_{\nu_2,\lambda_2}^{(\kappa_2)}(r_2) \times \left(\frac{r_<^q}{r_>^{q+1}}\right) S_{n_1,l_1}^{(k_1)}(r_1) S_{n_2,l_2}^{(k_2)}(r_2), \tag{19}$$

which can be decomposed into

TABLE VI. Triplet state resonances below I_4: our results on the left are compared with the results of [3]. The dimension of the matrices used to obtain these data was $n=11744$ and $p=6386$, respectively. The data presented were subject to a stability analysis with respect to varying values of the complex rotation angle θ.

$-\mathrm{Re}(E_{i,\theta})$	$-\mathrm{Im}(E_{i,\theta})$	$-\mathrm{Re}(E_{i,\theta})$	$-\mathrm{Im}(E_{i,\theta})$
This work		Bürgers *et al.* [3]	
0.169306634	0.000021005	0.169306635	0.000021006
0.161480663	0.000051983	0.161480663	0.000051980
0.15212204	0.00001680	0.152122029	0.000016799
0.15117642	0.00002241	0.151176420	0.000022408
0.14716881	0.00003711	0.147168813	0.000037116
0.14317600	0.00001140	0.143175987	0.000011381
0.14169136	0.00001470	0.141691356	0.000014696
0.14008854	0.00000439	0.140088484	0.000004409
0.13999805	0.00002018	0.139998046	0.000020176
0.13796132	0.00000764	0.137961324	0.000007642
0.13678714	0.00000959	0.136787119	0.000009622
0.13597556	0.00000173	0.135975513	0.000001752
0.13585741	0.00001502	0.135857413	0.000015013
0.13467953	0.00000525	0.134679533	0.000005256
0.13381173	0.00000647	0.133811711	0.000006493
0.133329281	0.000001326	0.133329246	0.000001340
0.13323044	0.00001051	0.133230435	0.000010505
0.13249065	0.00000372	0.132490651	0.000003725
0.13184923	0.00000452	0.131849211	0.000004540
0.131533756	0.000001077	0.131533731	0.000001087
0.13145699	0.00000755	0.131456986	0.000007547
0.130962374	0.000002716	0.130962374	0.000002717
0.13048099	0.00000327	0.130480976	0.000003283
0.130261387	0.000000879	0.130261370	0.000000886
0.130202294	0.000005580	0.130202295	0.000005577
0.129855236	0.000002034	0.129855236	0.000002035
0.129487234	0.000002436	0.129487225	0.000002444
0.129327408	0.000000718	0.129327395	0.000000724
0.129281535	0.000004229	0.129281436	0.000004228
0.129028519	0.000001558	0.129028519	0.000001559
0.128742045	0.000001860	0.128742039	0.000001867
0.128621741	0.000000588	0.128621731	0.000000593
0.128585657	0.000003277	0.128585657	0.000003276
0.128395405	0.000001218	0.128395405	0.000001219
0.128168621	0.000001452	0.128168616	0.000001457
0.128075628	0.000000487	0.128075620	0.000000489
0.128046837	0.000002588	0.128046838	0.000002588
0.127900092	0.000000969	0.127900092	0.000000970
0.127717811	0.000001154	0.127717807	0.000001158
0.127644357	0.000000404	0.127644351	0.000000407
0.127621072	0.000002079	0.127621073	0.000002078
0.127505445	0.000000783	0.12750544	0.00000079
0.127356921	0.000000932	0.127356918	0.000000935

TABLE VI. (*Continued.*)

$-\mathrm{Re}(E_{i,\theta})$	$-\mathrm{Im}(E_{i,\theta})$	$-\mathrm{Re}(E_{i,\theta})$	$-\mathrm{Im}(E_{i,\theta})$
This work		Bürgers *et al.* [3]	
0.127297848	0.000000338	0.127297839	0.000000341
0.127278774	0.000001694	0.127278774	0.000001694
0.127186005	0.000000641	0.1271860	0.0000006
0.127063496	0.000000763	0.12706350	0.00000077
0.127015248	0.000000285	0.12701524	0.00000029
0.126999448	0.000001398	0.1269993	0.0000014
0.126923855	0.000000532		
0.126821690	0.000000634		
0.126781760	0.000000243		
0.12676853	0.00000117		
0.1267061	0.0000004		

$$U = \int_0^\infty dr_1 S^{(\kappa_1)}_{\nu_1,\lambda_1}(r_1) S^{(k_1)}_{n_1,l_1}(r_1) r_1^q \times \int_{r_1}^\infty dr_2 S^{(\kappa_2)}_{\nu_2,\lambda_2}(r_2) S^{(k_2)}_{n_2,l_2}(r_2) \frac{1}{r_2^{q+1}} + \int_0^\infty dr_2 S^{(\kappa_2)}_{\nu_2,l_2}(r_2) S^{(k_2)}_{n_2,l_2}(r_2) r_2^q \times \int_{r_2}^\infty dr_1 S^{(\kappa_1)}_{\nu_1,\lambda_1}(r_1) S^{(k_1)}_{n_1,l_1}(r_1) \frac{1}{r_1^{q+1}}. \quad (20)$$

The GL quadrature formula for these integrals involves double sums over a number of integration points which are determined by the degree of the polynomial part of the subintegral functions (for details see, e.g., [38]). If $n_1^{\max}$ and $n_2^{\max}$ are the maximum values of the radial indices of the Sturmian functions of the electrons 1 and 2 involved in the whole basis, respectively, then by choosing the number of integration points $N_{ij}=n_1^{\max}+n_2^{\max}+1$ for GL integration allows the computation of all matrix elements [Eq. (20)]. With this choice all double sums have the same length N_{ij}^2 that scales quadratically with the sum of $n_1^{\max}$ and $n_2^{\max}$. The description of highly excited states requires rather large values of $n_1^{\max}$ and $n_2^{\max}$ for which this choice turns out to be rather inefficient as briefly mentioned below in Sec. IV. Alternatively one might adjust the number of integration points to each of the integrals [Eq. (20)], which would imply to calculate the integrations points (zeros of Laguerre polynomials) several times. However, this is even less efficient.

To reduce the number of operations needed to compute the matrix representation of $1/r_{12}$ we adopt a method, recently developed by Zamastil *et al.* [36,37], based on the generalized Wigner-Eckart theorem and recurrence relations. In the following, the method is reviewed and adjusted to our definition of Coulomb-Sturmian functions $S^{(k)}_{n,l}(r)$, which are connected to the Sturmian functions $R_{n,l}(kr)$ used in [37] by

$$R_{n,l}(kr) = C_n^{(k)} \frac{S^{(k)}_{n,l}(r)}{r}, \quad \text{with} \quad C_n^{(k)} = \sqrt{\frac{n}{k}}. \quad (21)$$

1. Linearization of the product of two Sturmian functions

The Wigner-Eckhart theorem for Sturmian functions [Eq. (49) of [37]] reads as [52]

$$S^{(k_i)}_{n_i,l_i}(r) S^{(\kappa_i)}_{\nu_i,\lambda_i}(r) = \sum_{N_i=L_i+1}^{\nu_i+n_i} (\nu_i,\lambda_i,\kappa_i,n_i,l_i,k_i|N_i) S^{(\xi_i)}_{N_i,L_i}(r), \quad (22)$$

with $\xi_i=\kappa_i+k_i$ and $L_i=\lambda_i+l_i$. Orthogonality relation (9) for the Sturmian functions leads to

$$(\nu_i,\lambda_i,\kappa_i,n_i,l_i,k_i|N_i) = \frac{N_i}{\xi_i} \int_0^\infty dr S^{(k_i)}_{n_i,l_i}(r) S^{(\kappa_i)}_{\nu_i,\lambda_i}(r) \frac{1}{r} S^{(\xi_i)}_{N_i,L_i}(r). \quad (23)$$

After substitution of the products of two Sturmian functions in the radial integrals of the $1/r_{12}$ matrix elements [Eq. (20)] by the corresponding expansions [Eq. (22)], we obtain

$$U = \sum_{N_1=L_1+1}^{\nu_1+n_1} \sum_{N_2=L_2+1}^{\nu_2+n_2} [\mathcal{G}^{L_1,L_2,q}_{N_1,N_2}(\xi_1,\xi_2) + \mathcal{G}^{L_2,L_1,q}_{N_2,N_1}(\xi_2,\xi_1)] \times (\nu_1,\lambda_1,\kappa_1,n_1,l_1,k_1|N_1)(\nu_2,\lambda_2,\kappa_2,n_2,l_2,k_2|N_2), \quad (24)$$

where $\mathcal{G}^{L_i,L_j,q}_{N_i,N_j}$ are the integrals defined by

$$\mathcal{G}^{L_i,L_j,q}_{N_i,N_j}(\xi_i,\xi_j) = \int_0^\infty dr_i S^{(\xi_i)}_{N_i,L_i}(r_i) r_i^q \int_{r_i}^\infty dr_j S^{(\xi_j)}_{N_j,L_j}(r_j) \frac{1}{r_j^{q+1}}. \quad (25)$$

The advantage of the transcription of Eq. (20) in terms of coefficient (23) and integral (25) is given through the possibility of an recursive computation of the involved coefficients as well as of the integrals.

2. Recurrence relation for the coefficients $(\nu_i,\lambda_i,\kappa_i,n_i,l_i,k_i|N_i)$

In case of fixed values for λ_i, κ_i, l_i, and k_i within an equation, we employ the shorthand notation

$$(\nu_i,n_i|N_i) = \sqrt{\frac{\kappa_i k_i}{\xi_i}} \sqrt{\frac{N_i}{\nu_i n_i}} (\nu_i,\lambda_i,\kappa_i,n_i,l_i,k_i|N_i). \quad (26)$$

These coefficients satisfy the recurrence relation [37]

$$\begin{aligned}\sqrt{(\nu_i-\lambda_i-1)(\nu_i+\lambda_i)}(\nu_i,n_i|N_i) &= 2\left(\nu_i-1-\frac{\kappa_i N_i}{\xi_i}\right)(\nu_i-1,n_i|N_i) \\ &- \sqrt{(\nu_i+\lambda_i-1)(\nu_i-\lambda_i-2)}(\nu_i-2,n_i|N_i) \\ &+ \frac{\kappa_i}{\xi_i}\sqrt{(N_i+L_i)(N_i-L_i-1)}(\nu_i-1,n_i|N_i-1) \\ &+ \frac{\kappa_i}{\xi_i}\sqrt{(N_i-L_i)(N_i+L_i+1)}(\nu_i-1,n_i|N_i+1). \end{aligned} \quad (27)$$

This equation can be used to lower the quantum number ν_i to λ_i+1. Taking into account that

$$(\nu_i,\lambda_i,\kappa_i,n_i,l_i,k_i|N_i) = (n_i,l_i,k_i,\nu_i,\lambda_i,\kappa_i|N_i) \tag{28}$$

provides the means to lower the quantum number n_i to l_i+1. The initial conditions for the recursion [Eq. (27)] are $(\nu_i^{(0)},n_i^{(0)}|N_i^{(0)})$ and $(\nu_i^{(0)},n_i^{(0)}|N_i^{(0)}+1)$, with $\nu_i^{(0)}=\lambda_i+1$, $n_i^{(0)}=l_i+1$, and $N_i^{(0)}=\lambda_i+l_i+1$. These have simple analytical expressions given by [37]

$$(\nu_i^{(0)},n_i^{(0)}|N_i^{(0)}) = 2(\lambda_i+l_i+1) \times \frac{\kappa_i^{\lambda_i+1}k_i^{l_i+1}}{(\kappa_i+k_i)^{\lambda_i+l_i+2}}\sqrt{\frac{(2\lambda_i+2l_i+1)!}{(2\lambda_i+1)!\,(2l_i+1)!}},$$

$$(\nu_i^{(0)},n_i^{(0)}|N_i^{(0)}+1) = -\sqrt{2(\lambda_i+l_i+1)} \times \frac{\kappa_i^{\lambda_i+1}k_i^{l_i+1}}{(\kappa_i+k_i)^{\lambda_i+l_i+2}}\sqrt{\frac{(2\lambda_i+2l_i+1)!}{(2\lambda_i+1)!\,(2l_i+1)!}}. \tag{29}$$

In addition it holds

$$(\nu_i^{(0)},n_i^{(0)}|N_i) = 0, \quad N_i > \lambda_i+l_i+2. \tag{30}$$

3. Recurrence relations for the integrals $\mathcal{G}_{N_i,N_j}^{L_i,L_j,q}(\xi_i,\xi_j)$

Equations (67) and (72) of [37] provide recurrence relations for the $\mathcal{G}_{N_i,N_j}^{L_i,L_j,q}(\xi_i,\xi_j)$ that keep the indices L_i, L_j, and q and the parameters ξ_1 and ξ_2 constant. After transforming these according to Eq. (21) we obtain

$$\begin{aligned}\langle N_1,L_1,\xi_1|N_2,L_2,\xi_2\rangle &= q\mathcal{G}_{N_1,N_2} + \frac{(N_2+L_2)}{2}\sqrt{\frac{(N_2-1)(N_2-L_2-1)}{N_2(N_2+L_2)}}\mathcal{G}_{N_1,N_2-1} \\ &\quad - \frac{(N_2-L_2)}{2}\sqrt{\frac{(N_2+1)(N_2+L_2+1)}{N_2(N_2-L_2)}}\mathcal{G}_{N_1,N_2+1},\end{aligned} \tag{31}$$

and

$$\begin{aligned}\langle N_1,L_1,\xi_1|N_2,L_2,\xi_2\rangle &= (q+1)\mathcal{G}_{N_1,N_2} \\ &\quad + \frac{(N_1-L_1)}{2}\sqrt{\frac{(N_1+1)(N_1+L_1+1)}{N_1(N_1-L_1)}}\mathcal{G}_{N_1+1,N_2} \\ &\quad - \frac{(N_1+L_1)}{2}\sqrt{\frac{(N_1-1)(N_1-L_1-1)}{N_1(N_1+L_1)}}\mathcal{G}_{N_1-1,N_2},\end{aligned} \tag{32}$$

respectively. Here we have employed—under the condition of a fixed set of parameters L_1, L_2, q, ξ_1, and ξ_2—the shorthand notation:

$$\mathcal{G}_{N_1,N_2} = \mathcal{G}_{N_1,N_2}^{L_1,L_2,q}(\xi_1,\xi_2). \tag{33}$$

In addition, Eqs. (31) and (32) include the overlap integral

$$\langle N_1,L_1,\xi_1|N_2,L_2,\xi_2\rangle = \int_0^\infty dr S_{N_1,L_1}^{(\xi_1)}(r)S_{N_2,L_2}^{(\xi_2)}(r). \tag{34}$$

These overlaps and the initial conditions for recursions (31) and (32) are calculated with GL integration. Notice that for $\xi_1=\xi_2$ the overlaps have simple analytical expressions which are implemented in our computations.

III. NUMERICAL TREATMENT

A. Computation of the matrix representation of the generalized eigenvalue problem

The matrix elements of the kinetic term and the electron-nucleus interaction of $\mathbf{H}_\theta$, and of the overlap matrix $\mathbf{S}$ are calculated using GL integration that guarantees an accuracy of the order of the machine precision (in double and quadruple precision). The matrix elements of $1/r_{12}$ can also be computed very accurately with GL integration, but Eq. (24) combined with recursive relations (27), (31), and (32) provides a much more efficient method. However, its implementation is delicate. Recursions (27), (31), and (32) are not numerically stable even for rather small values of N_i and L_i (e.g., $N_i-L_i>15$, $L_i>10$). Typically one observes a slow decay in precision at each recursion step up to a certain point, which is then followed by a rather rapid total breakdown of precision. Consequently, a computation of matrix elements of $1/r_{12}$ using purely the recursive method described in Sec. II C seems not to be feasible. To overcome the instability issues we limit the length of the recursions and restart the recursion process. The implementation is described in detail in the following.

To compute the coefficients $(\nu_i,n_i|N_i)$ the three-dimensional coefficient matrix is initialized to zero and decomposed into two dimensional slices with fixed ν_i. Using Eq. (29) the two initial values for the slice with $\nu_i=\lambda_i+1$ are then evaluated. Looking at Eq. (27) it is easy to spot that for $\nu_i=\lambda_i+1$ the nonzero coefficients are situated in the upper right triangle, the diagonal, and the first lower subdiagonal. These matrix elements are then computed columnwise, starting with the element of the first lower subdiagonal [see Fig. 1 (left)]. Analogously we compute the auxiliary matrix for $n_i=l_i+1$. From Eq. (28) follows that the coefficients with $n_i=l_i+1$ correspond to the initial conditions for the matrix slices with $\nu_i\neq\lambda_i+1$ [see Fig. 1 (center and right)]. The slices with $\nu_i\neq\lambda_i+1$ are computed in a similar way. The major difference in their computation is that after a number $\mathfrak{R}$ of columns computed via the recursion formula we compute two columns by using GL integration techniques and then restart the recursion for another "reclength" or $\mathfrak{R}$ columns [see Fig. 1 (right)]. In doing so we ensure that we are able to contain the loss of precision.

The matrix $\mathcal{G}_{N_i,N_j}$ is divided into blocks of dimension "blocklength" or $\mathfrak{B}$ (see Fig. 2). Displaced by two rows downwards with respect to the center of the block a set of four initial values is calculated by using GL integration methods. The displacement of the starting values is done as to be able to compute efficiently zero values for integrals with $N_i>N_j$ in the case of equal dilation parameters $\xi_i=\xi_j$. Starting from these the rest of the block is computed by employing recursion formulas (31) and (32). In doing so we are able to shorten the length of the recursion and ensure a certain level of precision.

The computations of the coefficients $(\nu_i,n_i|N_i)$ and the integrals $\mathcal{G}_{N_i,N_j}$ are performed in 128-bit arithmetic if neces-

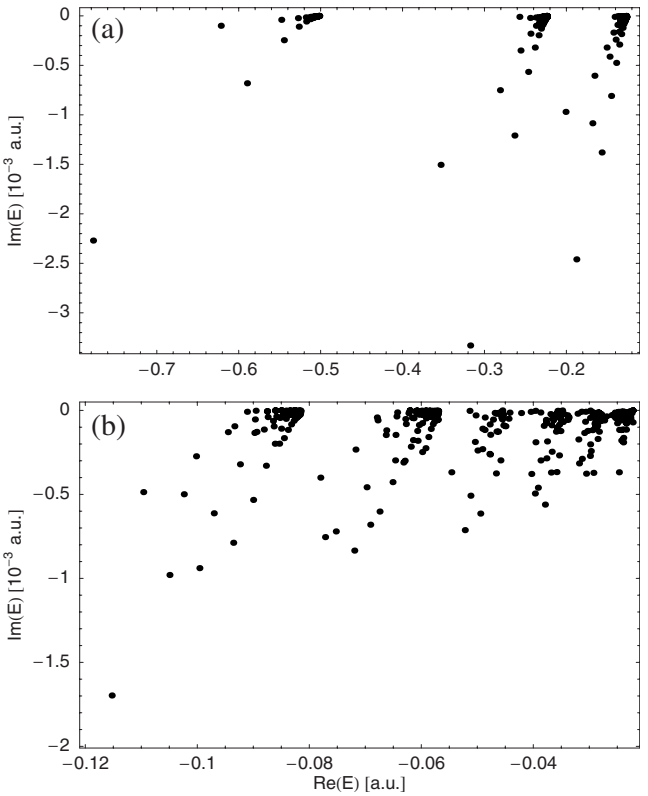

FIG. 3. Resonance spectrum for singlet symmetry $L=0$ states. (a) Shows the data presented in Tables I, III, and V. In (b) the converged resonances from above I_4 to below I_{10} are displayed. The used criterion of convergence was maximum relative deviation of the real part of 10^{-4} and maximum relative deviation of the imaginary part of 10^{-2} for at least three values of θ. The spectra have been obtained with matrices smaller or equal than $n=12\,240$ and $p=8778$, respectively.

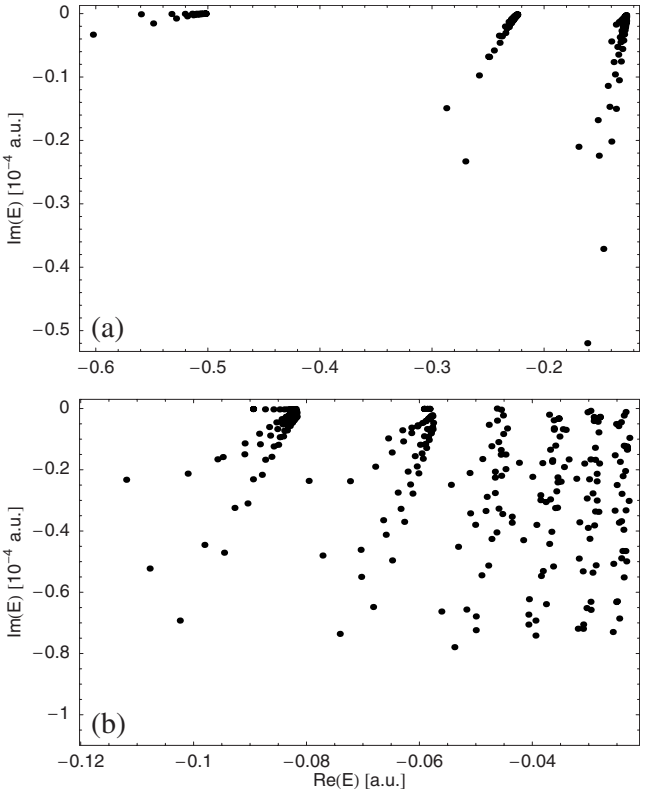

FIG. 4. Resonance spectrum for triplet symmetry $L=0$ states. (a) Shows the data presented in Tables II, IV, and VI. In (b) the converged resonances from above I_4 to below I_{10} are displayed. The used criterion of convergence was maximum relative deviation of the real part of 10^{-4} and maximum relative deviation of the imaginary part of 10^{-2} for at least three values of θ. The spectra have been obtained with matrices smaller or equal than $n=12\,240$ and $p=8278$, respectively. For the energy regime above I_5 the convergence of narrow resonances ($K=-N+1$) is limited due to the smallness of the imaginary part of the eigenvalues in comparison with the real part.

sary converted to other precision and then used to compute matrix elements of $1/r_{12}$ as given by Eqs. (11) and (24). The parameters $\mathfrak{R}$ and $\mathfrak{B}$ are optimized to yield the desired precision by as few GL integrated elements as possible, e.g., to ensure 26 digits of accuracy $\mathfrak{R}=6$ and $\mathfrak{B}=10$ are sufficient, while $\mathfrak{R}=18$ and $\mathfrak{B}=26$ provide at least 15 digits of accuracy for coefficients and integrals ($L_i, L_j < 50$, $N_i - L_i$, $N_j - L_j < 100$, and $0.02 \leq \xi_i, \xi_j \leq 4.00$).

B. Solution of the eigenvalue problem

The inclusion of many sets of Coulomb-Sturmian functions with different dilation parameters in our basis makes it numerically overcomplete, which means that some eigenvalues of the overlap matrix (which must be positive definite) can be zero or even negative. This results from a loss of numerical independence due to finite precision arithmetic. In order to solve this problem we proceed as follows. Let $\mathbf{H}_\theta$ and $\mathbf{S}$ be $(n \times n)$ matrices, and let us consider the $(n \times n)$ orthogonal matrix $\mathbf{T}$ that diagonalizes $\mathbf{S}$. Therefore, $\mathbf{T}^\mathsf{T}\mathbf{S}\mathbf{T}=\mathbf{s}$, where $\mathbf{s}$ is the diagonal matrix containing the eigenvalues of $\mathbf{S}$ of which the associated eigenvectors are stored in columns of $\mathbf{T}$. We define a small cutoff ϵ (of the order of 10^{-12}) and reject all eigenvalues of $\mathbf{S}$ that are smaller than this cutoff. We denote by p the number of overlap eigenvalues that are greater or equal to the cutoff. By rejecting the n-p overlap eigenvalues and their corresponding eigenvectors, the sizes of $\mathbf{T}$ and $\mathbf{s}$ are reduced to $(n \times p)$ and $(p \times p)$, respectively. Using basic matrix algebra, one can show that Eq. (18) can be transformed into the ordinary eigenvalue problem

$$\tilde{\mathbf{H}}_\theta \tilde{\mathbf{\Psi}}^{L,M}_{i,\theta} = E_{i,\theta} \tilde{\mathbf{\Psi}}^{L,M}_{i,\theta}, \tag{35}$$

with

$$\tilde{\mathbf{H}}_\theta = \mathbf{V}^\mathsf{T}\mathbf{H}\mathbf{V},$$

$$\tilde{\mathbf{\Psi}}^{L,M}_{i,\theta} = \mathbf{V}^{-1}\mathbf{\Psi}^{L,M}_{i,\theta}, \tag{36}$$

where $\tilde{\mathbf{H}}_\theta$ is a $(p \times p)$ matrix, $\tilde{\mathbf{\Psi}}^{L,M}_{i,\theta}$ is a $(p \times 1)$ vector, and $\mathbf{V}$ is a $(n \times p)$ matrix given by

TABLE VII. Singlet state resonances below I_6 and actual precision; the dimension of the matrices used to obtain these data was $n=11808$ and $p=6193$, respectively. The used criterion of convergence was maximum relative deviation of the real part of 10^{-4} and maximum relative deviation of the imaginary part of 10^{-2} for at least three values of θ.

$-\mathrm{Re}(E_{i,\theta})$	$-\mathrm{Im}(E_{i,\theta})$	$-\mathrm{Re}(E_{i,\theta})$	$-\mathrm{Im}(E_{i,\theta})$
0.07803	0.00040	0.0592650	0.0000218
0.077179	0.000755	0.0592493	0.0002250
0.075259	0.000724	0.05924720	0.00000099
0.07197	0.00083	0.0591693	0.0000474
0.071751	0.000233	0.05903087	0.00000400
0.069767	0.000456	0.058739	0.000158
0.069113	0.000680	0.0587098	0.0000314
0.067934	0.000042	0.05870388	0.00000155
0.067803	0.000059	0.0586368	0.0000295
0.067454	0.000601	0.0585482	0.0000027
0.066339	0.000146	0.0583035	0.0001101
0.066252	0.000119	0.0582713	0.0000023
0.065135	0.000427	0.0582679	0.0000382
0.0646766	0.0002976	0.058214	0.000019
0.0646037	0.0001459	0.05815259	0.00000639
0.0644329	0.0000361	0.0579425	0.0000813
0.0643087	0.0000122	0.0579212	0.0000024
0.063202	0.000310	0.0579127	0.0000421
0.062962	0.000300	0.0578718	0.0000108
0.0628546	0.0000515	0.05782639	0.00000857
0.0627563	0.0000814	0.0576439	0.0000640
0.06229723	0.00001692	0.05763370	0.00000235
0.06205363	0.00000056	0.05755575	0.00000868
0.061872	0.000216	0.0574577	0.0000197
0.0616514	0.0000441	0.0573948	0.0000022
0.061491	0.000177	0.0573938	0.0000378
0.061377	0.000047	0.0573937	0.0000580
0.0609470	0.0000141	0.05732928	0.00000769
0.06084037	0.00000096	0.0572486	0.0000144
0.060732	0.000123	0.05719414	0.00000207
0.060650	0.000181	0.0571939	0.0000285
0.0604259	0.0000869	0.0571928	0.0000580
0.060350	0.000026	0.05713818	0.00000645
0.0599835	0.0000140	0.0570707	0.0000108
0.05993838	0.00000137	0.0570269	0.0000552
0.0598501	0.0000758	0.05702415	0.00000195
0.059850	0.000248	0.0570228	0.0000220
0.0596356	0.0000284	0.05697575	0.00000537
0.0595730	0.0000115		

$$\mathbf{V} = \mathbf{T}\mathbf{s}^{-1/2}. \tag{37}$$

The numerical diagonalization of the eigenvalue problem [Eq. (35)] is performed by an efficient implementation of the Lanczos algorithm [53–55].

TABLE VIII. Real and imaginary parts of few selected resonances below I_{10}. The dimension of the matrices used to obtain these data was $n=12240$ and $p=8548$, respectively. The used criterion of convergence was maximum relative deviation of the real part of 10^{-4} and maximum relative deviation of the imaginary part of 10^{-2} for at least three values of θ.

$-\mathrm{Re}(E_{i,\theta})$	$-\mathrm{Im}(E_{i,\theta})$	$-\mathrm{Re}(E_{i,\theta})$	$-\mathrm{Im}(E_{i,\theta})$
−0.0239821	−0.0000061	−0.0233936	−0.0000775
−0.023951	−0.000190	−0.023265	−0.000062
−0.023929	−0.000163	−0.0231951	−0.0000558
−0.0238002	−0.000345	−0.0230812	−0.0000105
−0.0236262	−0.0000606	−0.0229936	−0.0000248
−0.023619	−0.000025	−0.022926	−0.000062
−0.0235660	−0.0000303	−0.0228979	−0.0000073
−0.0235573	−0.0000713	−0.0228237	−0.0000075
−0.023441	−0.000116	−0.022682	−0.000051
−0.0233989	−0.0000122	−0.022672	−0.000042

IV. RESULTS

The described spectral method and the computation of matrix elements of $1/r_{12}$ via the restarted recursion method have been used to compute highly doubly excited states of helium for singlet and triplet symmetries. We have chosen to compute resonances for $L=0$ as these states contain the highest degree of symmetry, which makes them converge slower in this CI approach. The previously described spectral method is applicable to any value of the total angular momentum and should give better convergence for higher values of L, which has already been illustrated in [7] for singly excited states.

In order to compute the spectra up to the tenth SIT we have used one choice of parameter sets for each regime between two SITs and for each symmetry. Each basis expansion consists of an expansion into 16 angular configurations and five sets $[k_{1s},N_{1s}^{\min},N_{1s}^{\max},k_{2s},N_{2s}^{\min},N_{2s}^{\max}]$ for each angular configuration. Up to the fifth ionization threshold the dilation parameters are, by a rule of thumb, chosen to be $k_{1s}=2/N$ and $k_{2s}=2/n_s$, where N and n_s are the excitations of the inner and the outer electron of the resonance to describe, respectively. The n_s are taken as such that they account for different excitation of the outer electron in order to allow a description of a whole energy regime. The values of $N_{is}^{\min},N_{is}^{\max}$ $(i=1,2)$ are then chosen to provide an interval around N and n_s, respectively, i.e., $N_{1s}^{\min}<N<N_{1s}^{\max}$ and $N_{2s}^{\min}<n_s<N_{2s}^{\max}$. In general the number of Sturmians introduced for the inner electron is larger for symmetric excitation of both electrons than in the case of a very asymmetric configuration. For the higher-lying thresholds the choice of the dilation parameters has to be amended as they have to account for different series and screening effects.

To take care of the numerical overcompleteness of the basis the $(n\times n)$ matrices $\mathbf{H}_\theta$ and $\mathbf{S}$ are transformed into the basis where the overlap is diagonal. The transformation matrix consists of the eigenvectors of the overlap matrix associated to eigenvalues larger than the cutoff $\epsilon=10^{-12}$, resulting

in an effective reduction in the Hamiltonian matrix into an $(p \times p)$ matrix (see Sec. III B) which has then to be diagonalized.

The computation of matrix elements of $1/r_{12}$ with GL integration techniques is rather cumbersome and renders the optimization of the basis for an energy regime extremely time consuming and therefore limits the described approach. The implementation of the computation of $1/r_{12}$ via the restarted recursion method reduces computation time tremendously and allows for an application of this spectral method to the computation of highly doubly excited states of helium. Several performance tests have been done. For instance, we have computed the matrix representation of $1/r_{12}$ for a matrix designed to describe the resonance spectrum below the sixth SIT with both methods on an ITANIUM2 processor at the Linux Cluster of the Leibniz-Rechenzentrum of the Bayerische Akademie der Wissenschaften. The computation time reduces from 22.5 h for pure GL integration to slightly less than 2 h for the method described in Sec. III A. Moreover, the speedup of this method compared to GL integration increases with increasing maximum radial and angular indices of the included Coulomb-Sturmian functions.

Tables I–VI display the real and imaginary parts of resonances up to below I_4. Only converged digits are shown. In Tables I, III, and V our results for the singlet symmetry spectra below I_2 to below I_4 are compared to reference data from [3], while in Tables II, IV, and VI our results for triplet symmetry are again presented together with data from [3]. The presented data has been tested for convergence with respect to variation of the complex rotation angle θ, the dilation parameters, and the number of angular configurations. For a given choice of the parameters $[k_{1s}, N_{1s}^{\min}, N_{1s}^{\max}, k_{2s}, N_{2s}^{\min}, N_{2s}^{\max}]$ several values of θ in the interval $[0.085,0.2]$ have been chosen. Note that the data presented in Tables I–VI have each been obtained with one optimized basis choice with an effective dimension of the resulting matrix of $p<8500$ for singlet and $p<8000$ for triplet symmetry. In contrast, the results in [3] where obtained using perimetric coordinates and the typical basis dimensions were three times larger for the results presented up to the fourth SIT and about a factor 5 larger for convergence around the ninth ionization threshold [56].

In the case of singlet symmetry the data in Tables I, III, and V show a precision of five to eight significant digits for the real part and around two significant digits for the imaginary part of the resonance energies. For triplet symmetry (see Tables II, IV, and VI) the accuracy is around nine significant digits for the real part and two significant digits for the imaginary part, respectively. The discrepancy between the precision for singlet and triplet symmetries is due to the influence of the Kato cusp [57], which is a discontinuity of the derivative of the wave function at $r_{12}=0$ that is not resolvable within our approach. In the case of triplet symmetry the influence of the Kato cusp is softened by the Pauli principle. With increasing excitation of the outer electron the number of converged digits rises in general in contrast to the EC approach in [3]. This is due to the fact that the Kato cusp is more important for symmetrically excited configurations. Along Tables I–VI some resonances converge better than others, which is a signature that the basis is more ideal for the description of such resonances. Indeed, the convergence of single states depends a lot on the used basis, a clear example therefore is the triplet I_3 ground state, which converges better than anticipated from the above argument, which is most probably a consequence of an almost ideal basis for the description of this state. The precision for a single resonance can be vastly improved by optimizing the basis for this state instead of optimizing the basis for an energy regime.

In Figs. 3 and 4 the spectra up to I_{10} are displayed for singlet and triplet symmetries, respectively. For resonances above the fourth SIT the criterion of convergence is given through a coincidence of eigenenergies for at least three different values of the complex rotation angle θ with a maximum relative deviation of 10^{-4} of the real part and 10^{-2} of the imaginary part. The criterion is designed to exclude the discretized continuum states, numerical artifacts, and nonconverged resonances in an efficient manner and does not reflect the actual accuracy of the computed resonances, which is in most cases significantly higher. To show the actual precision of our results we give apart from the graphical data in Figs. 3 and 4 the energy and half width for converged resonances below the sixth and tenth thresholds in Tables VII and VIII (only converged digits are displayed), respectively. Notice that in Table VIII we present the resonances in a narrow energy window which by far are not all found converged resonances. Nevertheless, the results presented in Tables VII and VIII have not been published so far, as much as we know of, and can thus be considered as benchmark results. Triplet state resonances with extremely narrow width, which are usually members of the $K=-N+1$ series, do often not suffice the above-mentioned criterion as for these resonances we usually obtain only one to two significant digits for the imaginary part. This is clearly visible in Fig. 4, where for the energy regime above the fifth SIT only few members of these series are visible. Note that the largest matrices to diagonalize in order to obtain these spectra were of dimension $p=8778$ for singlet and $p=8278$ for triplet symmetry and are thus significantly smaller than in state-of-the-art methods.

V. SUMMARY

We presented an implementation for an efficient computation of matrix elements of $1/r_{12}$ within our CI approach. The implementation is based on a combination of a linearization of the product of two Coulomb-Sturmian functions, recurrence relations, and Gauss-Laguerre integration techniques. The method reduces the computation time by at least a factor of 10 compared with pure GL integration and renders an optimization of the basis for doubly excited states possible. Comparison of the spectrum of singlet and triplet S states up to the fourth ionization threshold with existing data shows the accuracy of our calculations obtained with a rather small effective basis size which did not exceed 9000. In addition we provided energies and widths of the resonances converging to the sixth and tenth SITs. Our results show that the computation of highly doubly excited states is possible

within our CI approach even in the energy regime where mixing of series for different ionization thresholds and overlapping resonances occur. Therefore, our approach might also help to shed some light in the understanding of this region of the spectrum where signatures of the underlying mixed regular and chaotic dynamics of the atom are expected to become observable, such as Ericsson fluctuations in the photoionization cross section [12,21], loss of approximate quantum numbers [9,12], or semiclassical scaling laws for the photoionization cross section below the double ionization threshold [58].

Furthermore, this approach is equally valid for the description of the spectrum of the manifolds with any value of the total angular momentum L. Therefore, it makes a treatment of the driven system possible and thus opens up a possibility for the search for nondispersive wave packets and gives perspectives in the treatment of multiphoton ionization processes, in particular in the low-frequency regime.

ACKNOWLEDGMENTS

The authors are indebted to Yuri Popov for bringing [36] to their attention and for many interesting discussions. They also thank Jaroslav Zamastil for sending them Maple sheets of the implementation of his recursive procedure for computing $1/r_{12}$ and Dominique Delande for fruitful discussions. The work was supported by the Deutsche Forschungsgemeinschaft, Contract No. FR 591/16-1. J.M. thanks the "Fonds de la Recherche Scientifique de la Communauté Francaise de Belgique" for his post doctotal position at the Université catholique de Louvain under the convention 4.4.503.02.F I.I.S.N.

[1] R. P. Madden and K. Codling, Phys. Rev. Lett. **10**, 516 (1963).
[2] C. D. Lin, Phys. Rep. **257**, 1 (1995).
[3] A. Burgers, D. Wintgen, and J.-M. Rost, J. Phys. B **28**, 3163 (1995).
[4] B. Grémaud and D. Delande, Europhys. Lett. **40**, 363 (1997).
[5] J. M. Rost, K. Schulz, M. Domke, and G. Kaindl, J. Phys. B **30**, 4663 (1997).
[6] G. Tanner, K. Richter, and J.-M. Rost, Rev. Mod. Phys. **72**, 497 (2000).
[7] E. Foumouo, G. L. Kamta, G. Edah, and B. Piraux, Phys. Rev. A **74**, 063409 (2006).
[8] O. Sinanoğlu and D. R. Herrick, J. Chem. Phys. **62**, 886 (1975).
[9] D. R. Herrick and O. Sinanoğlu, Phys. Rev. A **11**, 97 (1975).
[10] A. Czasch *et al.*, Phys. Rev. Lett. **95**, 243003 (2005).
[11] M. Domke, K. Schulz, G. Remmers, G. Kaindl, and D. Wintgen, Phys. Rev. A **53**, 1424 (1996).
[12] Y. H. Jiang, R. Püttner, D. Delande, M. Martins, and G. Kaindl, Phys. Rev. A **78**, 021401(R) (2008).
[13] G. Handke, M. Draeger, and H. Friedrich, Physica A **197**, 113 (1993).
[14] G. Handke, M. Draeger, W. Ihra, and H. Friedrich, Phys. Rev. A **48**, 3699 (1993).
[15] M. Draeger, G. Handke, W. Ihra, and H. Friedrich, Phys. Rev. A **50**, 3793 (1994).
[16] W. Ihra, M. Draeger, G. Handke, and H. Friedrich, Phys. Rev. A **52**, 3752 (1995).
[17] A.-T. Le, T. Morishita, X.-M. Tong, and C. D. Lin, Phys. Rev. A **72**, 032511 (2005).
[18] J. Xu, A.-T. Le, T. Morishita, and C. D. Lin, Phys. Rev. A **78**, 012701 (2008).
[19] J. Madroñero, P. Schlagheck, L. Hilico, B. Grémaud, D. Delande, and A. Buchleitner, Europhys. Lett. **70**, 183 (2005).
[20] K. Richter and D. Wintgen, Phys. Rev. Lett. **65**, 1965 (1990).
[21] J. Eiglsperger and J. Madroñero, Phys. Rev. A **80**, 022512 (2009).
[22] G. J. Madroñero Pabón, Dissertation, Ludwig-Maximilians-Universität München, 2004 (http://edoc.ub.uni-muenchen.de/archive/00002187).
[23] J. Madroñero and A. Buchleitner, Phys. Rev. A **77**, 053402 (2008).
[24] C. L. Pekeris, Phys. Rev. **112**, 1649 (1958).
[25] M. Rotenberg, Adv. At. Mol. Phys. **6**, 233 (1970).
[26] E. Huens, B. Piraux, A. Bugacov, and M. Gajda, Phys. Rev. A **55**, 2132 (1997).
[27] G. Lagmago Kamta, B. Piraux, and A. Scrinzi, Phys. Rev. A **63**, 040502(R) (2001).
[28] L. Feng and H. W. van der Hart, Phys. Rev. A **66**, 031402(R) (2002).
[29] L. Feng and H. W. van der Hart, J. Phys. B **36**, L1 (2003).
[30] C. W. McCurdy, D. A. Horner, T. N. Rescigno, and F. Martín, Phys. Rev. A **69**, 032707 (2004).
[31] S. Laulan and H. Bachau, Phys. Rev. A **69**, 033408 (2004).
[32] P. Antoine, E. Foumouo, B. Piraux, T. Shimizu, H. Hasegawa, Y. Nabekawa, and K. Midorikawa, Phys. Rev. A **78**, 023415 (2008).
[33] T. Nubbemeyer, K. Gorling, A. Saenz, U. Eichmann, and W. Sandner, Phys. Rev. Lett. **101**, 233001 (2008).
[34] J. S. Parker, B. J. S. Doherty, K. T. Taylor, K. D. Schultz, C. I. Blaga, and L. F. DiMauro, Phys. Rev. Lett. **96**, 133001 (2006).
[35] J. S. Parker, K. J. Meharg, G. A. McKenna, and K. T. Taylor, J. Phys. B **40**, 1729 (2007).
[36] J. Zamastil, J. Čížek, M. Kalhous, L. Skála, and M. Šimánek, J. Math. Phys. **45**, 2674 (2004).
[37] J. Zamastil, F. Vinette, and M. Šimánek, Phys. Rev. A **75**, 022506 (2007).
[38] G. Lagmago Kamta, Ph.D. thesis, Université Nationale du Bénin, 1999.
[39] D. A. Varschalovich, A. N. Moskalev, and V. K. Khersonskii, *Quantum Theory of Angular Momentum* (World Scientific, Singapore, 2008).
[40] This relation does not mean that the parity of a given state depends on the angular momentum L. In fact, this relation defines the parity of the states that are actually coupled by the dipole interaction Hamiltonian.
[41] J. Aguilar and J. M. Combes, Commun. Math. Phys. **22**, 269 (1971).
[42] E. Balslev and J. M. Combes, Commun. Math. Phys. **22**, 280

(1971).
[43] B. Simon, Ann. Math. **97**, 247 (1973).
[44] W. P. Reinhardt, Annu. Rev. Phys. Chem. **33**, 223 (1982).
[45] Y. Ho, Phys. Rep. **99**, 1 (1983).
[46] S. Graffi, V. Grecchi, and H. J. Silverstone, Ann. Inst. Henri Poincaré, Sect. A **42**, 215 (1985).
[47] M. Reed and B. Simon, *Methods of Modern Mathematical Physics: Analysis of Operators* (Academic, New York, 1978), Vol. IV.
[48] M. Pont and R. Shakeshaft, Phys. Rev. A **43**, 3764 (1991).
[49] A. Bohm, M. Gadella, and G. B. Mainland, Am. J. Phys. **57**, 1103 (1989).
[50] L. D. Landau and E. M. Lifschitz, *Lehrbuch der Theoretischen Physik: III Quantenmechanik* (Akademie-Verlag Berlin, 1979).
[51] M. Abramowitz and I. Stegun, *Handbook of Mathematical Functions* (Dover, New York, 1972).
[52] The coefficients [Eq. (27)] are accordingly related to the coefficients $(\nu_i,\lambda_i,\kappa_i,n_i,l_i,k_i|N_i)_{p=1}$ of [37] through the relation $(\nu_i,\lambda_i,\kappa_i,n_i,l_i,k_i|N_i)=\sqrt{\frac{\kappa_i k_i}{\xi_i}}\sqrt{\frac{N_i}{\nu_i n_i}}(\nu_i,\lambda_i,\kappa_i,n_i,l_i,k_i|N_i)_{p=1}$.
[53] C. Lanczos, J. Res. Natl. Bur. Stand. **45**, 255 (1950).
[54] B. N. Parlett and D. S. Scott, Math. Comput. **33**, 217 (1979).
[55] T. Ericsson and A. Ruhe, Math. Comput. **35**, 1251 (1980).
[56] B. Grémaud, Thèse de Doctorat, Université Paris 6, 1997.
[57] C. C. J. Roothaan and A. W. Weiss, Rev. Mod. Phys. **32**, 194 (1960).
[58] C. W. Byun, N. N. Choi, M.-H. Lee, and G. Tanner, Phys. Rev. Lett. **98**, 113001 (2007).